Evidence for the interior evolution of Ceres from geologic analysis of fractures

J. E. C. Scully[1]*, D. L. Buczkowski[2], N. Schmedemann[3], C. A. Raymond[1], J. C. Castillo-Rogez[1], S. D. King[4], M. T. Bland[5], A. I. Ermakov[1], D. P. O'Brien[6], S. Marchi[7], A. Longobardo[8], C. T. Russell[9], R. R. Fu[10], and M. Neveu[11].

[1]Jet Propulsion Laboratory, California Institute of Technology, 4800 Oak Grove Drive, Pasadena, California 91109, USA, [2]Johns Hopkins University Applied Physics Laboratory, Laurel, Maryland 20723, USA, [3]Freie Universität Berlin, 12249 Berlin, Germany, [4]Virginia Tech, Blacksburg, Virginia 24061, USA, [5]US Geological Survey, Astrogeology Science Center, Flagstaff, Arizona 86001, USA, [6]Planetary Science Institute, Tucson, Arizona 85719, USA, [7]Southwest Research Institute, Boulder, Colorado 80305, USA, [8]INAF Istituto di Astrofisica e Planetologia Spaziali (IAPS), 00133 Rome, Italy, [9]Department of Earth, Planetary, and Space Science, University of California, Los Angeles, California 90095, USA, [10]Lamont-Doherty Earth Observatory, Columbia University, Palisades, New York 10964, USA, [11]Arizona State University, Tempe, AZ 85287, USA.

*Corresponding author: Jennifer E. C. Scully (jennifer.e.scully@jpl.nasa.gov)

Key Points:

- We identify all ≥1 km wide linear features outside impact craters: most are secondary crater chains and there is one set of pit chains.

- Pit chains are the surface expression of subsurface fractures and they reveal the localized outer layer is thicker than Ceres' average.
- We propose a region of upwelling material, resulting from convection/diapirism, formed the pit chains and we derive its characteristics.

Abstract

Ceres is the largest asteroid-belt object and has been observed by the Dawn spacecraft since 2015. Dawn observed two morphologically distinct linear features on Ceres' surface: secondary crater chains and pit chains. Pit chains provide unique insights into Ceres' interior evolution. Pit chains called the Samhain Catenae are interpreted as the surface expression of subsurface fractures. Using their spacing, we estimate that the localized thickness of Ceres' fractured, outer layer is approximately ≥58 km, at least ~14 km greater than average. We hypothesize that the Samhain Catenae were formed by extensional stresses induced by a region of upwelling material resulting from convection/diapirism. We derive characteristics for this upwelling material that can be used as constraints in future interior modeling studies. For example, its predicted location coincides with Hanami Planum, a high-elevation region with negative residual gravity anomaly, which may be surficial evidence for this proposed region of upwelling material.

1. Introduction

Prior to the Dawn mission [*Russell et al.,* 2016], dwarf planet Ceres (radius ~470 km) was studied via telescopic observations and modeling investigations. Telescopic observations allowed for the initial determination of Ceres' dimensions and average bulk density, and provided evidence for at least partial differentiation [*Thomas et al.*, 2005; *Drummond et al.* 2014]. Thermal evolution models predicted Ceres differentiated into a rocky interior and a 50-100 km thick water-ice-dominated outer layer [*Castillo-Rogez and McCord,* 2010; *McCord and Sotin,* 2005], within which extensive viscous relaxation was predicted to occur [*Bland,* 2013]. Alternatively, arguments were also made for an undifferentiated interior [*Zolotov,* 2009].

A deeper understanding of Ceres' interior required orbital observations, which were provided by Dawn and refine Ceres' dimensions and bulk density [*Russell et al.,* 2016]. They

also indicate partial differentiation into a rock-rich interior and an outer layer that is comparatively enriched in volatiles [*Park et al.,* 2016]. Dawn obtained images with two to three orders of magnitude higher resolution than previous telescopic observations: ≥35 m/pixel [*Buczkowski et al.,* 2016] versus 30 km/pixel [*Li et al.,* 2006]. These images reveal a heavily cratered surface [*Hiesinger et al.,* 2016; *Marchi et al.,* 2016] that is inconsistent with the predicted extensive surficial viscous relaxation [*Bland,* 2013]. Furthermore, the surface morphology and finite element modeling indicate Ceres' outer layer is a mixture of <30-40% of a weak phase (water ice and porosity) and >60-70% rock/salts/clathrates [*Buczkowski et al.*, 2016; *Bland et al.,* 2016]. Dawn's high-resolution images also show numerous linear features on Ceres' surface [*Buczkowski et al.,* 2016].

2. Types of linear features and ejecta distribution

We investigate these linear features by producing a global map of all linear features that are ≥1 km wide and are outside of impact craters. The global map contains 2,319 individual segments and is based on images from Dawn's Framing Camera and the shape model of Ceres [*Roatsch et al.,* 2016; *Preusker et al.,* 2016] (Text S1-S2) (Figures 1, S1-S2). Using this global map, we identify two types of linear features: secondary crater chains and pit chains. While we use the pit chains to gain insights into Ceres' interior evolution, it is also necessary to study the secondary crater chains, to ensure that pit chains are not misidentified as secondary crater chains, and vice versa. We distinguish between the secondary crater chains and pit chains using the following morphologic characteristics. Secondary craters have more clearly defined rims and more regular shapes in comparison to the pits, and the chains of secondary craters are often (though not always) located in a radial pattern around a source impact crater. These characteristics are consistent with the formation of the secondary crater chains by the impact and

scour of material ejected during the formation of a central source impact crater (Text S3) (Figure 2). In contrast, the pits have poorly defined rims and more irregular shapes than the secondary craters, and the chains of pits are not located in a radial pattern around an impact crater. These characteristics are indicative of the pit chains forming by drainage of material into a subsurface void, and are analogous to pit chains on other bodies [*Wyrick et al.,* 2004; *Buczkowski et al.,* 2008; *Ferrill et al.,* 2011; *Scully et al.,* 2014; *Martin et al.,* 2017] (Text S6) (Figure 2). The secondary crater chains and pit chains also display different behaviors in color and spectral data [*De Sanctis et al.,* 2015], which is similar to other bodies [*Longobardo et al.,* 2015] (Text S7).

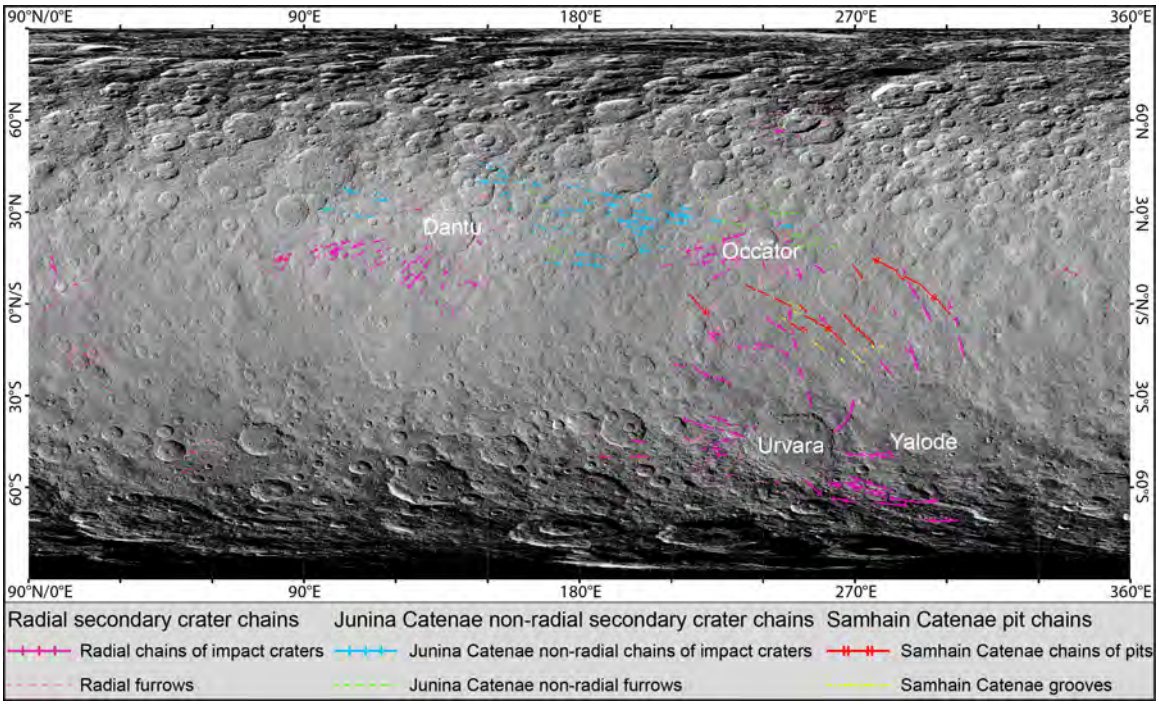

Figure 1. Global map of prominent linear features, classified by interpretation into radial secondary crater chains, Junina Catenae non-radial secondary crater chains and Samhain Catenae pit chains. Their sub-divisions are discussed in Text S2, S3 and S6 and in Figure 2. Impact craters discussed in the text are labeled. The basemap is an equirectangular projection of the Framing Camera LAMO clear filter global mosaic (35 m/pixel) (Text S1).

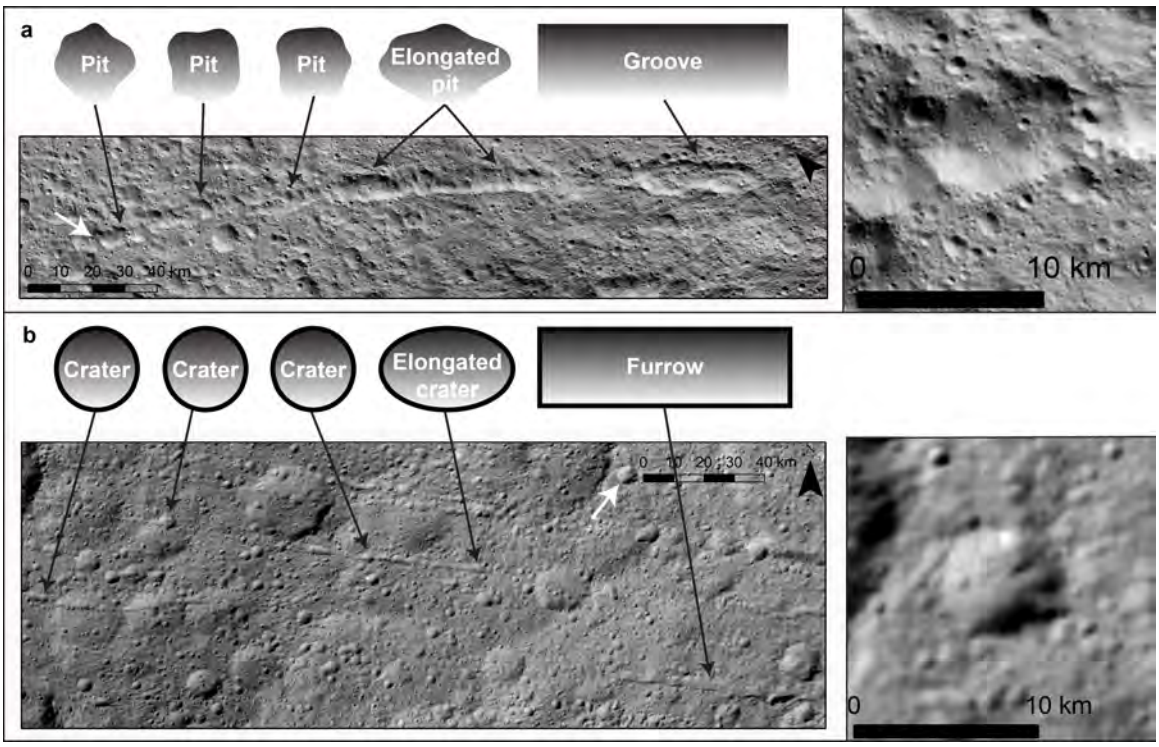

Figure 2. Schematic illustrations and examples of (**a**) pit chains and (**b**) secondary crater chains. Pit chains are made up of grooves (elongated pits) and chains of pits, which have more poorly defined rims and more irregular shapes than secondary craters (Text S2 and S6). (**b**) Secondary crater chains are made up of furrows (elongated impact craters) and chains of impact craters, which have more clearly defined rims and more regular shapes than pits (Text S2-S3). White arrows indicate the locations of the detailed images (right).

The majority of the linear features are radial secondary crater chains, which surround thirteen source impact craters. Those around Occator, Dantu and Urvara craters are the most prominent (Figures 1, S3-S4). However, one set of secondary crater chains, named the Junina Catenae, are not radial to a source impact crater. They are located from ~12-46°N and ~95-265°E, are oriented ~WNW-ESE, and consist of ~11 secondary crater chains that fan out to the west (Figures 1 and S5). Their average length is 491 km, their maximum/minimum widths are 4

118 km/1 km, their average depth is 230 m and their average spacing is 22 km. The Junina Catenae
119 are cross-cut by, and thus older than, Occator and Dantu craters and their associated radial
120 secondary crater chains (Figures 1, 3 and S5).

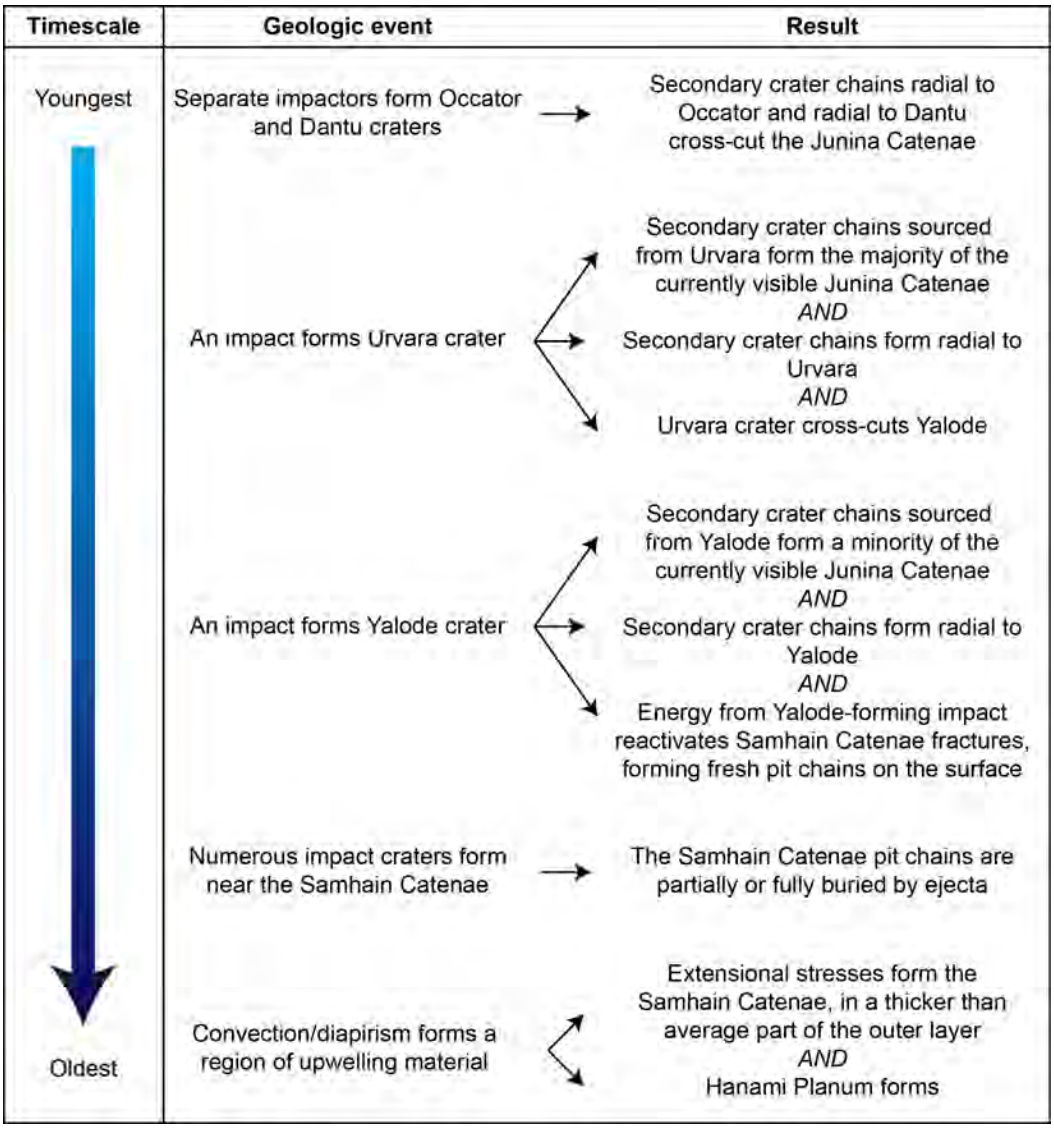

121

122 **Figure 3.** Timeline showing key events discussed in this work, from youngest to oldest. The
123 details are discussed in the text.

124

125 An ejecta distribution model explains how material ejected from Urvara crater, in the
126 southern hemisphere, formed the Junina Catenae in the northern hemisphere [*Schmedemann et*

127 *al.,* 2017] (Text S4). This model predicts that because of Ceres' low gravity (0.27 m/s^2), material
128 ejected at ~45° and at high velocities from Urvara (~390-520 m/s) will travel above Ceres'
129 surface for a relatively long time (~6-8 hours). In comparison to bodies like the Earth, Ceres'
130 rotation period is short (~9 hours) and it is small (radius ~470 km) [*Russell et al.,* 2016]. Thus,
131 by the time this material impacts the surface to form the Junina Catenae, the surface underneath
132 it has rotated significantly, resulting in the material being located far from Urvara in a non-radial
133 pattern. The model predictions of the location, orientation and fan pattern of this high velocity
134 material is consistent with our mapping of the Junina Catenae (Figure 4). A minority of the
135 currently visible Junina Catenae may have been formed by the impact of material originating
136 from Yalode crater, which is adjacent to, and older than, Urvara (Text S5). Also consistent with
137 our mapping, the model predicts that material ejected at lower velocities from Urvara will form
138 radial secondary crater chains (Text S5) (Figure S3). We also map additional, unnamed sets of
139 secondary crater chains that are not oriented radially around a source impact crater (Figure S2).
140 We propose that these sets formed by the same process as the Junina Catenae, but that they have
141 different source craters. Ejecta distribution modeling has not yet been performed to identify their
142 source craters.

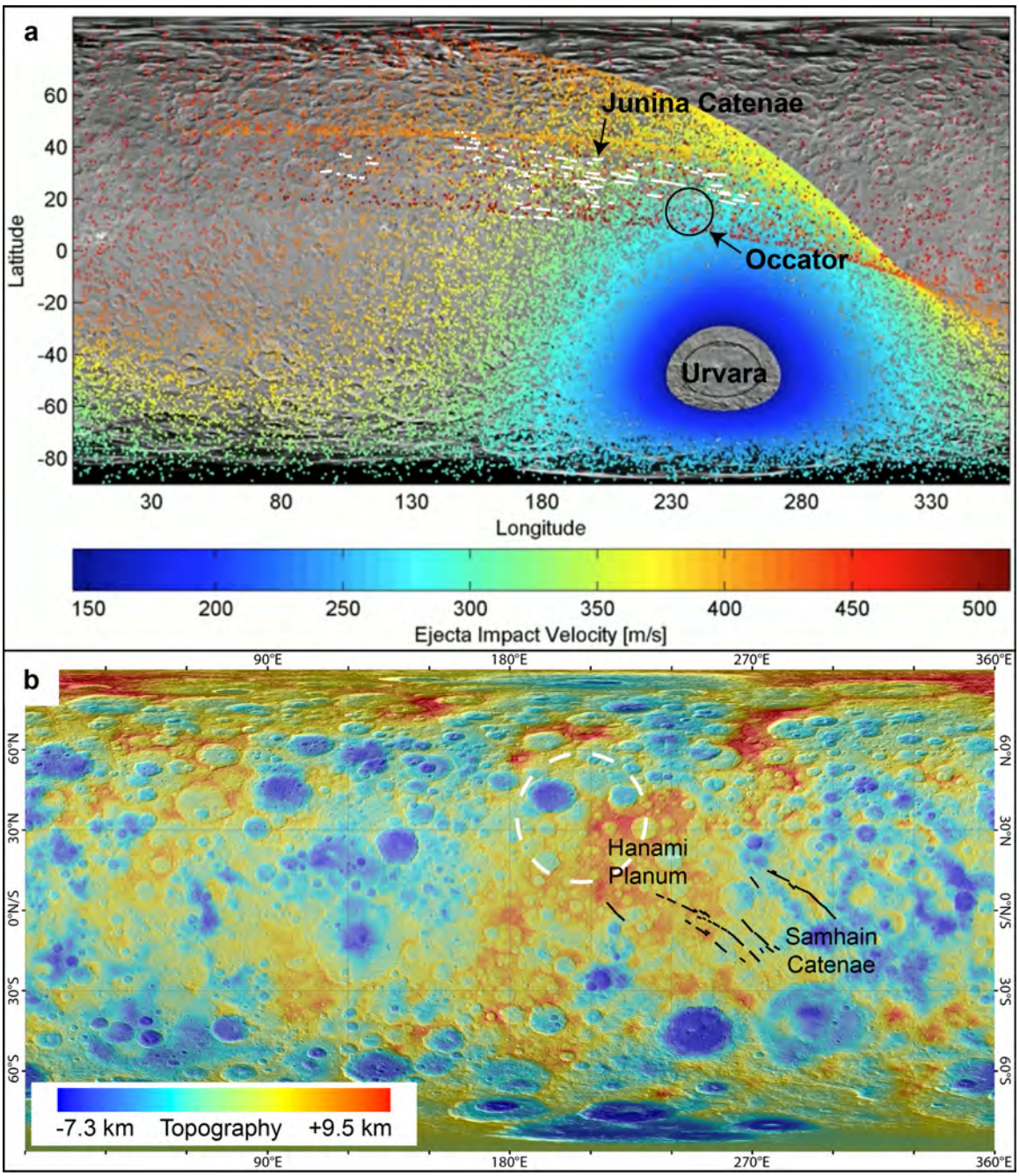

Figure 4. Formation of the Junina Catenae and Samhain Catenae. (**a**) Comparison between the predicted distribution of high velocity material ejected from Urvara [*Schmedemann et al.,* 2017] (red-orange dots) and our Junina Catenae mapping (white lines). (**b**) Locations of the Samhain Catenae (black lines), Hanami Planum and the proposed region of upwelling material (white

dashed circle). The basemap is the shape model overlain onto an equirectangular projection of the Framing Camera LAMO clear filter global mosaic (Text S1).

3. Samhain Catenae fractures and thickness of Ceres' outer layer

Another set of linear features, called the Samhain Catenae, are also not radial to a source impact crater (Figures 1 and 5). Unlike the Junina Catenae, we and *Buczkowski et al.* [2016] interpret that the Samhain Catenae are not secondary crater chains that originate from Urvara and/or Yalode, because they display the aforementioned morphological characteristics of pit chains (Text S6) (Figure 2). Additionally, the Samhain Catenae are aligned to the straight rims of polygonal craters, whose straight sides are hypothesized to be controlled by subsurface fractures [*Buczkowski et al.,* 2016] (Figure 5). Moreover, we observe that the Samhain Catenae are cross-cut by Urvara's and Yalode's secondary crater chains, indicating that they formed prior to Urvara and Yalode (Figures 3 and 5).

The Samhain Catenae are oriented ~NW-SE between Occator and Urvara/Yalode craters (Figure 1). They consist of ~6 discontinuous pit chains, with an average length of 202 km, a maximum/minimum width of 11 km/5 km and an average depth of 1.1 km (Figure 5). The Samhain Catenae are the only set of ≥1 km wide pit chains we identify on Ceres. Consistent with analogous pit chains on other bodies [*Wyrick et al.,* 2004; *Buczkowski et al.,* 2008; *Ferrill et al.,* 2011; *Scully et al.,* 2014; *Martin et al.,* 2017], we interpret that the Samhain Catenae pit chains are the surface expression of subsurface voids at depth. In this scenario, surficial material draining into a subsurface void forms a funnel-like shape in cross-section, which appears as a pit at the surface. We further interpret that extension fractures form these subsurface voids (Text S6).

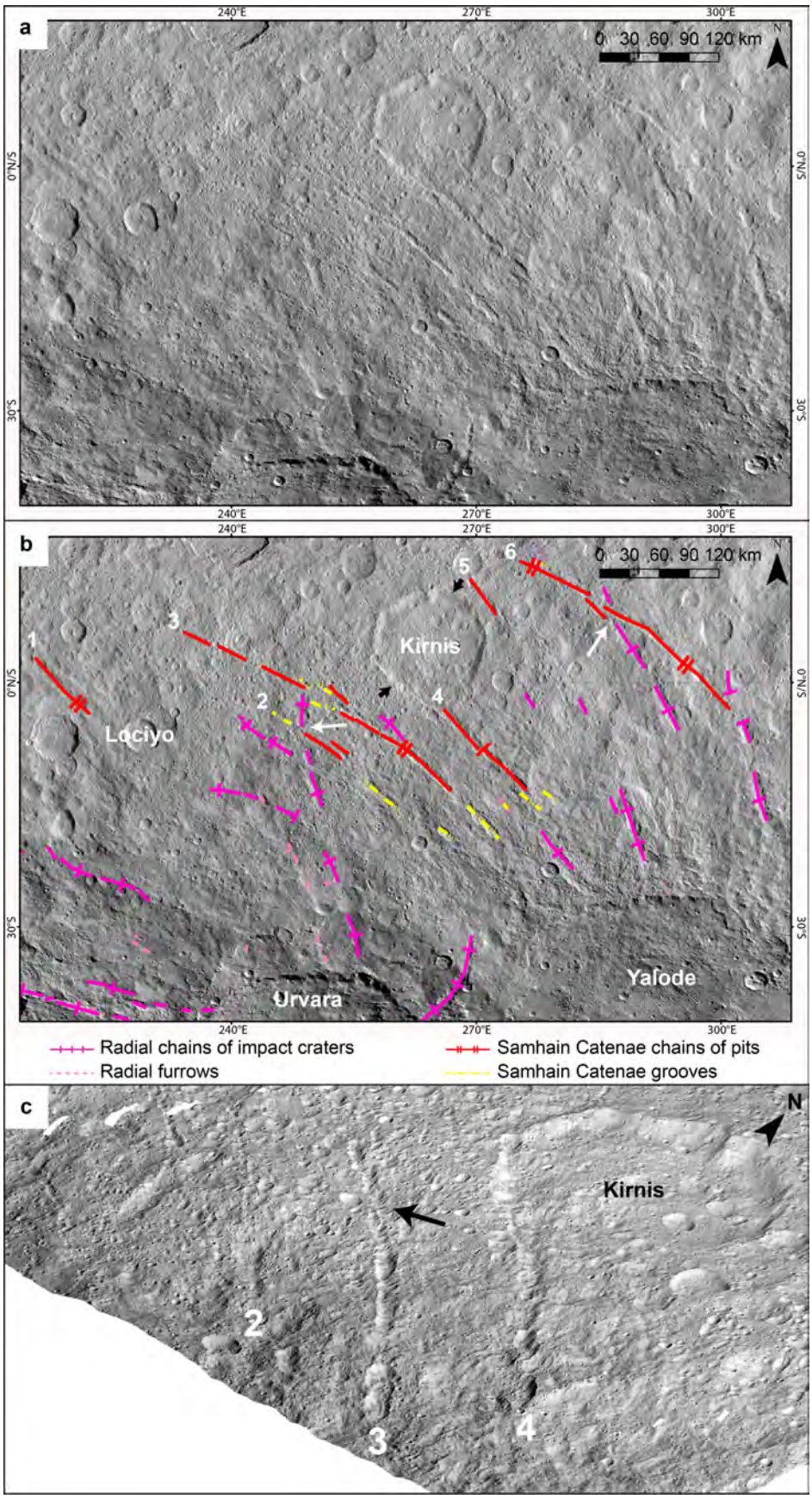
a
240°E
270°E
300°E
0°N/S
30°S
0 30 60 90 120 km
N
b
Kirnis
Lociyo
Urvara
Yalode
1
2
3
4
5
6
Radial chains of impact craters
Radial furrows
Samhain Catenae chains of pits
Samhain Catenae grooves
c
Kirnis
N
2
3
4

171

172 **Figure 5.** Samhain Catenae pit chains in (**a**) unmapped, (**b**) mapped and (**c**) perspective views.
173 (**b**) White arrows show example locations where Urvara/Yalode radial secondary crater chains
174 cross-cut the Samhain Catenae pit chains, which are labeled #1-6. Short black arrows indicate the
175 polygonal crater Kirnis' straight rims, which align with the Samhain Catenae. Kirnis' southern
176 straight rim merges with Samhain Catenae #4. The basemap is an equirectangular projection of
177 the Framing Camera LAMO clear filter global mosaic (Text S1). (**c**) Samhain Catenae #2-4 and
178 an example en-echelon pattern/S-shaped linkage (black arrow) (Text S6).
179
180 The spacing of tectonic features on planetary bodies is often used to estimate the
181 thicknesses of the layers in which they occur [e.g. *Gioia et al.*, 2007; *Yin et al.*, 2016; *Bland and*
182 *McKinnon*, 2015]. Numerical modeling and experiments show that the ratio of extension fracture
183 spacing to fractured layer thickness for fractures that have reached, or are near to, the level of
184 saturation is ~0.8-1.2 [*Bai and Pollard,* 2000]. The Samhain Catenae fractures, as indicated by
185 the pit chains at the surface, are likely near to saturation because their spacing is relatively
186 regular (Figure 5). The spacing between pit chains #1-2 is ~135 km, #2-3 is ~48 km, #3-4 is ~51
187 km, #4-5 is ~104 km and #5-6 is ~104 km. It is possible that additional fractures exist in the
188 subsurface, located centrally between #1-2, #4-5 and #5-6, which would result in a regular
189 spacing of ~50 km between all the fractures. Pit chains associated with these additional
190 subsurface fractures could have been concealed or erased from the surface by superposing
191 impact craters and their ejecta, such as Lociyo and Kirnis (Figure 5). However, because there is
192 no surficial morphological evidence for these additional subsurface fractures, in our calculations
193 we only use the spacings of the pit chains that are observed at the surface. Using the mean and
194 standard deviation of these spacings, and the aforementioned ratio of fracture spacing to

fractured layer thickness (~0.8-1.2), we estimate that the thickness of Ceres' fractured, outer layer in the localized region around the Samhain Catenae is ~58-134 km.

Estimates of Ceres' globally averaged outer layer thickness have been derived from interior models based on Dawn's gravity observations: $41.0^{+3.2}_{-4.7}$ km [*Ermakov et al.,* in revision; *Fu et al.,* in revision] and 43-50 km [*Mitri et al.,* in revision]. In contrast, our outer layer thickness estimate is only applicable to the vicinity of the Samhain Catenae. Thus, our results suggest that Ceres' outer layer in this region is thicker than the global average. This is consistent with *Ermakov et al.* [in revision], who suggest the outer layer is thickest in a region called Hanami Planum. The Samhain Catenae are located on and adjacent to Hanami Planum (Figure 4). By minimizing the power of the Bouguer anomaly, *Ermakov et al.* [in revision] estimate that the outer layer is ~55 km thick at Hanami Planum. This is comparable to our lower estimate of the outer layer thickness (~58 km). A regional outer layer thickness of ~58 km would be consistent with our aforementioned suggestion that there are additional subsurface fractures spaced at ~50 km. Thus, we interpret that our lower estimate, ~58 km, is most representative of Ceres' outer layer thickness in the vicinity of the Samhain Catenae. The gravity-derived outer layer thickness estimates reflect density differences between the outer layer and the underlying material, while our fracture-derived estimate reflects a rheology/strength difference. Therefore, the consistency between these outer layer thickness estimates in the vicinity of the Samhain Catenae suggests that the density and rheology/strength boundaries between the outer layer and underlying material occur at approximately the same depth in this region.

4. Reactivation and formation of the Samhain Catenae

Cross-cutting relationships indicate that Urvara and Yalode formed after the Samhain Catenae, and that Yalode is older than Urvara (Figures 3 and 5). It is likely that geologic events

after the Samhain Catenae fractures' formation, such as the deposition of ejecta from impact craters, would have partially or fully erased the initial pit chains from Ceres' surface. However, the observation that the Samhain Catenae pit chains closer to Yalode are deeper than the further pit chains (Figure S6) suggests that the large Yalode impact (260-km-diameter) reactivated the Samhain Catenae fractures. Reactivating/reopening the fractures at depth would result in new surficial material draining into the fractures, forming fresh pit chains on the surface that are visible as the Samhain Catenae today. The nearby 170-km-diameter Urvara crater could also have contributed to this reactivation.

Here we investigate three hypotheses for the formation of the Samhain Catenae being induced by: (1) a basin-forming impact, (2) freezing of a global subsurface ocean, or (3) a region of upwelling material. There is a geometric relationship between the Samhain Catenae and a putative relict impact basin at 20°N, 340°E [*Marchi et al.,* 2016], suggesting that stresses derived from the impact basin's formation could have initially formed the Samhain Catenae fractures. However, the geometric correlation is weak and the identification of this impact basin is ambiguous. Consequently, in agreement with *Buczkowski et al.* [2016], this is not our favored formation mechanism of the Samhain Catenae.

Alternatively, freezing of a global subsurface ocean could have formed the Samhain Catenae. In this scenario, the freezing ocean adds ice to the overlying outer layer, thickening and inducing tensile stresses in the outer layer [*O'Brien et al.,* 2015; *Nimmo,* 2004; *Manga and Wang,* 2007]. Dawn data indicate that Ceres' outer layer is mixture of water ice, rock, salts and/or clathrates [*Hiesinger et al.,* 2016; *Bland et al.,* 2016; *Castillo-Rogez et al.,* 2016]. We infer that such a mixture's tensile strength, without pre-existing weaknesses such as fractures, is at least an order of magnitude higher than pure water ice (≥10 MPa versus ~0.01-1 MPa),

because the tensile strength of water ice-silicate particle mixtures is ~2-22 MPa [*Petrovic,* 2003; *Lange and Ahrens,* 1983]. To fracture an outer layer with a tensile strength of ≥10 MPa, thickening of ≥10 km [*O'Brien et al.,* 2015] would be required, which could have occurred during freezing of a global subsurface ocean [*Castillo-Rogez et al.,* 2016]. However, if the Samhain Catenae fractures formed as a result of this freezing, we would expect them to be globally distributed, as on icy satellites [e.g. *Nimmo*, 2004; *Manga and Wang*, 2007]. It is possible that globally distributed fractures are buried on Ceres, and that only the Samhain Catenae portion were reactivated, and are hence visible today. However, there are approximately a dozen large impact craters (>100 km), in addition to Yalode (260-km-diameter) and Urvara (170-km-diameter), and none appear to have reactivated fractures. In particular, we would expect Kerwan crater's formation (280-km-diameter) to have reactivated other portions of any globally distributed fracture set. However, we find no pit chains of a similar scale to the Samhain Catenae elsewhere on Ceres. This suggests that globally distributed fractures are not present, and therefore, this is also not our favored formation mechanism of the Samhain Catenae.

The final hypothesis is that a region of upwelling material induced the Samhain Catenae's formation. Multiple interior evolution models predict convection approximately within Ceres' first billion years [*King et al.,* 2016; *Neveu and Desch,* 2015; *Travis and Feldman,* 2016]. Some models predict that convection continued after Ceres' first billion years, initially in the liquid state and perhaps later in the solid state [*Neveu and Desch,* 2015; *Travis and Feldman,* 2016]. Additionally, upwelling of salt diapirs is proposed to occur in the geologically recent past [*Buczkowski et al.,* 2016]. Thus, we hypothesize that a region of upwelling material derived from one of these instances of convection/diapirism induced extensional stresses within a particular portion of Ceres' outer layer, and formed the Samhain Catenae. Further modeling studies are

needed to evaluate this hypothesis, and our analysis of the Samhain Catenae provides predictions about the proposed region of upwelling material's characteristics, which can be used as constraints by future interior modeling studies.

5. Characteristics of the proposed region of upwelling material

The proposed upwelling would have occurred before Urvara's and Yalode's formation, because we find that the Samhain Catenae are older than both craters. Additionally, the upwelling material would need to induce extensional stresses within Ceres' outer layer that are greater than our previously approximated value of the outer layer's tensile strength (≥10 MPa). Furthermore, to form the Samhain Catenae, the extensional stresses induced in Ceres' outer layer would need to be approximately perpendicular to the Samhain Catenae's current orientation.

Dike swarms are often used to locate terrestrial mantle plumes because their patterns are indicative of the plume's location [*Ernst and Buchan,* 2001] (Figure S7). A dike is essentially a fracture that is infilled with material, and both are formed by tensile stresses/extension. Therefore, if the proposed region of upwelling material did form the Samhain Catenae, we can use the patterns of dikes formed by mantle plumes on Earth as analogs to the pattern of the Samhain Catenae, and thus approximate the location of the proposed region of upwelling material. Dikes/fractures with a linear pattern are approximately parallel to one another, have a higher density nearer to the upwelling material and their average thickness increases with distance from the upwelling material [*Ernst and Buchan,* 2001] (Figure S7). The Samhain Catenae are approximately parallel to one another, there are six pit chains in their northern half and four in their southern half (Figure S6), and by measuring the widths of the pit chains at regular intervals, we find that the average widths of five of the six pit chains are greatest at their southern ends. Therefore, we find that the Samhain Catenae have a linear pattern, which is

consistent with the proposed region of upwelling material being located adjacent to the northwestern end of the Samhain Catenae, at ~36°N, ~207°E (Figure 4).

6. Conclusions

Through our detailed analysis of Ceres' linear features, we find that the Samhain Catenae are the only ≥1 km wide pit chains on Ceres' surface. The remaining linear features are secondary crater chains formed by material ejected from nearby and distant impact craters. The Samhain Catenae's spacing indicates that Ceres' outer layer in their vicinity is approximately ≥58 km thick. This is at least ~14 km thicker than the global average. It is also consistent with gravity-derived interior model estimations of variations in the outer layer thickness [*Ermakov et al.,* in revision], and thus provides independent confirmation for this model. Additionally, we hypothesize that the Samhain Catenae were formed as the result of a region of upwelling material derived from convection or diapirism. We find the characteristics of this proposed region of upwelling material, which can be used as constraints in future modeling studies of Ceres' interior evolution. For example, we approximate its location to be ~36°N, ~207°E. This broadly coincides with Hanami Planum, which is a topographically high region with a negative residual gravity anomaly. A subsurface buoyancy-driven anomaly combined with a high rigidity/thick outer layer is one possible formation mechanism of Hanami Planum [*Ermakov et al.,* in revision]. Consequently, Hanami Planum may be evidence for the proposed region of upwelling material, and the Samhain Catenae may represent surficial evidence for past interior activity.

Acknowledgments, Samples, and Data

Part of the research was carried out at the Jet Propulsion Laboratory (JPL), California Institute of Technology, under a contract with the National Aeronautics and Space Administration. We thank the Dawn Flight Team at JPL for the development, cruise, orbital insertion and operations of the Dawn spacecraft at Ceres. We thank the instrument teams at the Max Planck Institute, German Aerospace Center (DLR), Italian National Institute for Astrophysics (INAF) and Planetary Science Institute (PSI) for the acquisition and processing of Dawn data. The Framing Camera data and shape model upon which we base our mapping are available on the PDS Small Bodies Node website at http://sbn.pds.nasa.gov/data_sb/missions/dawn.

References

Bai, T. and Pollard, D. D. (2000), Fracture spacing in layered rocks: a new explanation based on the stress transition, *J. Struct. Geol.*, *22*, 43-57.

Bland, M. T. (2013), Predicted crater morphologies on Ceres: Probing internal structure and evolution, *Icarus, 226*, 510-521.

Bland, M. T., and McKinnon, W. B. (2015), Forming Ganymede's grooves at smaller strain: Toward a self-consistent local and global strain history for Ganymede, *Icarus, 245,* 247-262.

Bland, M. T., et al. (2016), Composition and structure of the shallow subsurface of Ceres revealed by crater morphology, *Nat. Geosci., 9,* 538-542.

Buczkowski, D. L., Barnouin-Jha, O. S. and Prockter, L. M. (2008), 433 Eros lineaments: Global mapping and analysis, *Icarus*, *193,* 39-52.

333 Buczkowski, D. L., et al. (2016), The geomorphology of Ceres, *Science, 353 (6303)*, 1004.
334 Castillo-Rogez, J. C. and McCord, T. B. (2010) Ceres' evolution and present state constrained by
335 shape data, *Icarus, 205*, 443-459.
336 Castillo-Rogez, J. C., et al. (2016), Loss of Ceres' Icy Shell from Impacts: Assessment and
337 Implications, *Lunar Planet. Sci. Conf.*, *47*, 3012.
338 De Sanctis, M. C., et al. (2015), Ammoniated phyllosilicates with a likely outer Solar System
339 origin on (1) Ceres, *Nature*, *528*, 241-244.
340 Drummond, J. D., et al. (2014), Dwarf planet Ceres: Ellipsoid dimensions and rotational pole
341 from Keck and VLT adaptive optics images, *Icarus, 236*, 28-37.
342 Ermakov, A. I., et al. (in revision), Constraints on Ceres' internal structure and evolution from its
343 shape and gravity measured by the Dawn spacecraft, *J. Geophys. Res*. *This manuscript
344 is included with this submission. We expect it would be published before this paper
345 would be accepted but if it were not, we would substitute this reference with a 2017
346 LPSC abstract on the same topic.
347 Ernst, R. E., and Buchan, K. L. (2001), The use of mafic dike swarms in identifying and locating
348 mantle plumes, *Geological Society of America*, Special Paper 352.
349 Ferrill, D. A., Wyrick, D. Y. and Smart, K. J. (2011), Coseismic, dilational-fault and extension-
350 fracture related pit chain formation in Iceland: Analog for pit chains on Mars,
351 *Lithosphere*, *3,* 133-142.
352 Fu, R. R., et al. (in revision), The Interior Structure of Ceres as Revealed by Surface
353 Topography, *Earth Planet. Sc. Lett.* *This manuscript is included with this submission.
354 We expect it would be published before this paper would be accepted but if it were not,
355 we would substitute this reference with a 2016 AGU abstract on the same topic.

356 Gioia, G., Chakraborty, P., Marshak, S. and Kieffer, S. W. (2007), Unified model of tectonics
357 and heat transport in a frigid Enceladus, *P. Natl. Acad. Sci.*, *104,* 13578-13581.
358 Hiesinger, H., et al. (2016), Cratering on Ceres: Implications for its crust and evolution. *Science*,
359 *353,* aaf4759-1-8.
360 King, S. D., et al. (2016), 3D Spherical Convection Modeling of the Interior of Ceres, *Lunar*
361 *Planet. Sci. Conf., 47,* 1699.
362 Lange, M. A. and Ahrens, T. J. (1983), The Dynamic Tensile Strength of Ice and Ice-Silicate
363 Mixtures, *J. Geophys. Res., 88*, 1197-1208.
364 Li, J.-Y., et al. (2006), Photometric analysis of 1 Ceres and surface mapping from HST
365 observations, *Icarus*, *182,* 143-160.
366 Longobardo, A., et al. (2015), Mineralogical and spectral analysis of Vesta's Gegania and
367 Lucaria quadrangles and comparative analysis of their key features, *Icarus, 259*, 72-90.
368 Manga, M. and Wang, C.-Y. (2007), Pressurized oceans and the eruption of liquid water on
369 Europa and Enceladus, *Geophys. Res. Lett.*, *34*, L07202-1-5.
370 Marchi, S., et al. (2016), The missing large impact craters on Ceres, *Nat. Comm., 7 (12257)*, 1-9.
371 Martin, E. S., et al. (2017), Pit chains on Enceladus signal the recent tectonic dissection of the
372 ancient cratered terrains, *Icarus, 294,* 209-217.
373 McCord, T. B. and Sotin, C. (2005), Ceres: Evolution and current state. *J. Geophys. Res., 110*,
374 E050091-1-14.
375 Mitri, G., et al. (in revision), Crustal Structure and Internal Differentiation of the Dwarf Planet
376 Ceres, *Icarus*. *This manuscript is included with this submission. We expect it would be
377 published before this paper would be accepted but if it were not, we would substitute this
378 reference with a 2017 EGU abstract on the same topic.

379 Neveu, M. and Desch, S. J. (2015), Geochemistry, thermal evolution, and cryovolcanism on
380 Ceres with a muddy ice mantle, *Geophys. Res. Lett.*, *42*, 10197-10206.
381 Nimmo, F. (2004), Stress generated in cooling viscoelastic shells: Application to Europa, *J.*
382 *Geophys. Res., 109,* E12001-1-10.
383 O'Brien, D. P., et al. (2015), The Potential for Volcanism on Ceres Due to Crustal Thickening
384 and Pressurization of a Subsurface Ocean, *Lunar Planet. Sci. Conf.*, *46,* 2831.
385 Park, R. S., et al. (2016), A partially differentiated interior for (1) Ceres deduced from its gravity
386 field and shape, *Nature, 537,* 515-517.
387 Petrovic, J. J. (2003), Review – Mechanical properties of ice and snow, *J. Mater. Sci.*, *38*, 1-6.
388 Preusker, F., et al. (2016), Dawn at Ceres – Shape Model and Rotational State, *Lunar Planet. Sci.*
389 *Conf.*, *47*, 1954.
390 Roatsch, Th., et al. (2016), High-resolution Ceres High Altitude Mapping Orbit atlas derived
391 from Dawn Framing Camera images, *Planet. Space Sci., 129*, 103-107.
392 Russell, C. T., et al. (2016), Dawn arrives at Ceres: Exploration of a small, volatile-rich world,
393 *Science*, *353*, 1008-1010.
394 Schmedemann, N., et al. (2017), The Distribution of Impact Ejecta on Ceres, *Lunar Planet. Sci.*
395 *Conf., 48,* 1233.
396 Scully, J. E. C., et al. (2014), Geomorphology and structural geology of Saturnalia Fossae and
397 adjacent structures in the northern hemisphere of Vesta, *Icarus, 244,* 23-40.
398 Thomas, P. C., et al. (2005), Differentiation of the asteroid Ceres as revealed by its shape,
399 *Nature, 437,* 224-226.
400 Travis, B. J. and Feldman, W. C. (2016), Ceres Model Suggests Large Scale Topography May
401 Reflect Early Time Internal Convection, *Lunar Planet. Sci. Conf.*, 47, 2762.

Wyrick, D., et al. (2004), Distribution, morphology, and origins of Martian pit crater chains, *J. Geophys. Res., 109,* E06005-1-20.

Yin, A., et al. (2016), Mechanics of evenly spaced strike-slip faults and its implications for the formation of tiger-stripe fractures on Saturn's moon Enceladus, *Icarus*, *266,* 204-216.

Zolotov, M. Y. (2009), On the composition and differentiation of Ceres, *Icarus*, *204,* 183-193.